

## COMBUSTION CHARACTERISTICS OF COAL GANGUE AND BIOMASS UNDER AN O<sub>2</sub>/CO<sub>2</sub> ATMOSPHERE

by

**Zhen GONG, Changzhong SONG\*, Yuanyuan LI, Ze LI, and Xiangru JIA**

College of Energy and Power Engineering,  
Inner Mongolia University of Technology, Hohhot, China

Original scientific paper  
<https://doi.org/10.2298/TSCI191012061G>

*Oxygen concentration and biomass content are key factors of the combustion of a mixed sample of biomass and coal gangue. Herein, we studied the effect of oxygen concentration and biomass content and their corresponding combustion and kinetic characteristics. Experiments were conducted in a thermogravimetric analyzer under an O<sub>2</sub>/CO<sub>2</sub> atmosphere. Results showed that the fixed carbon combustion temperature, ignition temperature, and exothermic peak temperature decreased with oxygen concentration increased. By contrast, the burning rate of volatilization increased with oxygen concentration increased. The total and maximum loss rates of the sample, the burnout temperature, the exothermic peak temperature, and the comprehensive combustion index S gradually increased. As oxygen concentration increased, the activation energy at the initial stage of combustion gradually decreased, whereas the activation energy at the end of the reaction gradually increased when the oxygen concentration increased. Activation energy could be rapidly reduced after a small amount of biomass was added, whereas the biomass content had no significant influence on the activation energy of the samples at the end of combustion.*

Key words: *thermogravimetric analyzer, coal gangue, biomass, kinetic*

### Introduction

One of the technologies for carbon efficiency and storage is oxyfuel technology, which is also known as O<sub>2</sub>/CO<sub>2</sub> combustion technology that features high carbon capture efficiency and reduces pollutant emission [1-4]. Oxyfuel technology is considered one of the most promising CO<sub>2</sub> capture technologies because it can directly retrofit existing burners, and a high CO<sub>2</sub> concentration in burners can significantly improve the desulfurization rate [5, 6].

Biomass has the characteristics of large output, wide distribution, and strong recyclability. Biomass, which mainly includes byproducts of agricultural and forestry production processes, possesses a low ash content and a high volatile content [7-9]. Biomass combustion and photosynthesis are reversible processes of carbon transport, and almost no CO<sub>2</sub> emissions occur in the whole process. Therefore, the rational use of biomass reduces not only the use of fossil energy but also the emission of CO<sub>2</sub>. Biomass also have a mitigating global greenhouse effect with low CO<sub>2</sub> emissions.

The CO<sub>2</sub> emissions are efficiently reduced by biomass combustion and oxyfuel technologies. Thus, a combination of oxyfuel technology and biomass utilization for low C emission is crucial and has been widely explored. Tahmasebi *et al.* [10] conducted experiments on lignite

\* Corresponding author, e-mail: songchzh@imut.edu.cn

and microalgae and showed that the mass loss rate of microalgae increases as oxygen concentration increase, and thermogravimetric (TG) and derivative thermogravimetric (DTG) curves of brown coal combustion shift to a low temperature zone. Kayahan and Ozdogan [11] studied the mixed combustion and pollutant emission characteristics of biomass and lignite by using a fluidized bed of 30 kW/h. They showed that oxyfuel increases fuel-N conversion and SO<sub>2</sub> formation, and CO<sub>2</sub> concentration in flue gas reaches up to 23% in 30% oxygen enriched co-combustion. Kazanc *et al.* [12] and Riaza *et al.* [13] investigated the emission characteristics of biomass and coal-mixed combustion pollutants.

Coal gangue (CG) is an undesired but inevitable byproduct of coal mining and washing. In addition, this material has become one of the largest industrial wastes [14], which contain a high ash content, a low volatile content, and a low calorific value [15]. The massive accumulation of CG causes serious pollution soil and water sources because of the presence of more metal elements, such as Al, Fe, Ca, K, Mg, Pb, Hg, Cd, and Cr [16]. The CG has a certain calorific value, and spontaneous combustion and smoldering may occur when temperature is high. Therefore, CG will be harmful to the environment if it is not dealt with accordingly.

The CG and biomass are complementary in nature. The mixed combustion of CG and biomass can alleviate environmental problems caused by the long-term accumulation of CG in open air and reduce the use of fossil energy to alleviate the current situation of global energy shortage. The mixed combustion of biomass and CG in air atmosphere has been extensively investigated [17-20].

The combustion characteristics of fuel under an O<sub>2</sub>/CO<sub>2</sub> atmosphere are quite different from those under an air atmosphere because the chemical properties of CO<sub>2</sub> and N<sub>2</sub> are quite different. However, studies on the mixed combustion of CG and biomass under O<sub>2</sub>/CO<sub>2</sub> are still lacking. Herein, we mainly aimed to investigate the combustion and kinetic behavior of CG and biomass in an O<sub>2</sub>/CO<sub>2</sub> atmosphere through thermogravimetric analysis (TGA) and provide a theoretical basis for rationally using CG and biomass in an oxygen-rich atmosphere.

## Experiment

### Additional instructions

The CG used in the experiment was from the coal field in Xilinhot in Inner Mongolia in China, and the biomass was corn stalk (CS) from Inner Mongolia in China. The test samples were crushed, pulverized, and sieved to have a particle size of 120 mesh to 140 mesh (average particle size 0.1155 mm). The samples was subjected to proximate analysis by using an SDLA 718 instrument, and ultimate analysis was performed using an SDCHN 435 element analyzer and a YX-DL/A8500 sulfur analyzer, and An SDC 313 calorimeter was utilized to determine the heating value of the cartridge, tab. 1.

**Table 1. Proximate analysis and elemental analysis of the samples**

Sample	Proximate analysis [%]				Elemental analysis [%]					$Q_{\text{net}}$ [MJkg <sup>-1</sup> ]
	$M_{\text{ad}}$	$A_{\text{ad}}$	$FC_{\text{ad}}$	$V_{\text{ad}}$	$C_{\text{ad}}$	$H_{\text{ad}}$	$N_{\text{ad}}$	$O_{\text{ad}}$	$S_{\text{ad}}$	
CG	0.81	53.61	32.69	12.89	34.07	1.37	0.41	8.64	1.09	11.3
CS	1.89	8.50	17.84	71.69	44.23	5.64	1.17	38.30	0.19	16.76

Note: ad – air dry basis,  $M$  – moisture,  $A$  – ash,  $FC$  – fixed carbon,  $V$  – volatile,  $Q_{\text{net}}$  – heating value of cartridge,  
 $O_{\text{ad}} = 100\% - (C_{\text{ad}} + H_{\text{ad}} + N_{\text{ad}} + S_{\text{ad}} + A_{\text{ad}} + M_{\text{ad}})$

The samples were scanned and analyzed by using a Hitachi S-3400N SEM combined with an energy spectrometer. The SEM image of 2.00k times and energy spectrum analysis results are shown in fig. 1 and tab. 2, respectively.

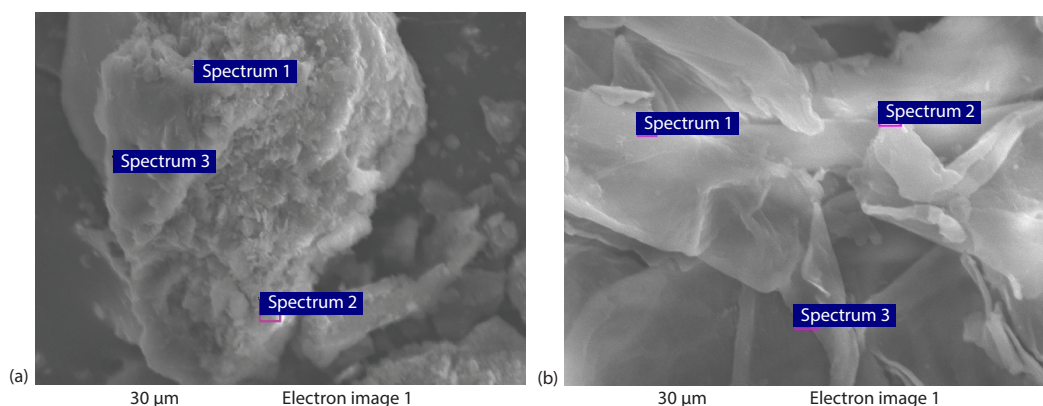


Figure 1. The SEM image of samples; (a) CG, (b) CS

Table 2. Energy spectrum analysis result of the samples [%]

Samples	Spectrum	C	O	Mg	Al	Si	S	Cl	K	Ca	Fe	Zr	Pt
CG	1		74.14		6.71	17.79	0.26		0.49		0.43		0.18
	2		57.57		5.75	16.66	11.25		0.61		6.99	1.17	
	3	44.40	43.45		5.62	5.87			0.46				0.20
CS	1	63.93	34.80	0.50				0.17	0.16	0.19		0.25	
	2	59.79	39.24	0.43		0.11		0.13	0.08	0.12			0.10
	3	69.01	29.23	0.63		0.34			0.21	0.31		0.18	0.09

Note: The content of each element in the table is atomically proportion

The SEM image showed that the surface of CS has obvious irregularities, and the surface and internal porosity are high. The CG particles are obvious, and the surface and internal porosity are low. The results of energy spectrum analysis, in addition C and O elements, CG contains some elements, such as Al, Si, S, K, Fe, Zr, and Pt. The contents of Al, Si, and Fe are higher than those of the other elements. The contents of C and O in the three positions of CS are higher than those of the other elements. The sum of the atomic proportions of the two was over 98%.

### Methods

In this study, the sample was tested using a NETZSCH STA449F5 synchronous thermal analyzer equipped with a TG-thermal difference (DSC) sensor, and TG and DSC changes in the samples were simultaneously measured. The schematic of the experimental device is shown in fig. 2.

This work mainly aimed to investigate the effect of the oxygen concentration and biomass content on the combustion characteristics of the samples under the O<sub>2</sub>/CO<sub>2</sub> atmosphere. In the test, first purge gas is O<sub>2</sub>, second purge gas and

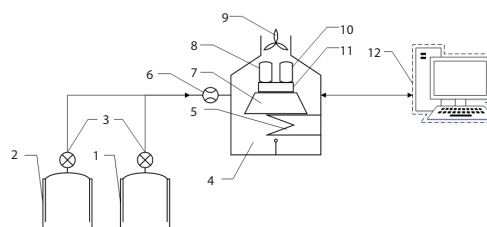


Figure 2. Schematic of a TG analyzer device; 1 – purge gas cylinder, 2 – protective gas cylinder, 3 – pressure reducing valve, 4 – furnace, 5 – programmed heating device, 6 – flow controller, 7 – thermal balance, 8 – fuel crucible, 10 – contrast crucible, 11 – heat flow sensor, and 12 – computer

shielding gas are CO<sub>2</sub>, the total flow rate of the three gases is 100 mL per minute, the pressure is 0.1 MPa, the mass of each sample is 10±0.5 mg, the heating rate is 20 °C per minute, and the temperature range is 40-1000 °C.

## Results and discussion

### *Thermogravimetry experiment*

#### *Combustion test with different oxygen concentrations under the O<sub>2</sub>/CO<sub>2</sub> atmosphere*

Combustion experiments were conducted in the atmosphere of 21% O<sub>2</sub>/79% CO<sub>2</sub> (21% O<sub>2</sub>), 30% O<sub>2</sub>/70% CO<sub>2</sub> (30% O<sub>2</sub>), 40% O<sub>2</sub>/60% CO<sub>2</sub> (40% O<sub>2</sub>), 50% O<sub>2</sub>/50% CO<sub>2</sub> (50% O<sub>2</sub>), and 60% O<sub>2</sub>/40% CO<sub>2</sub> (60% O<sub>2</sub>), and all the samples were mixed with a biomass content of 20%.

#### Analysis of TG and DTG characteristics

Figure 3 shows the TG and DTG curves of the samples with different oxygen concentrations. The TG curve and the DTG curve of the samples are similar at different oxygen concentrations. The DTG curve has an obvious loss peak at about 220 °C, 300 °C, and 500 °C, respectively, and the smallest loss peak is detected at 220 °C. The peak at 300 °C is lower than that at 220 °C, and the largest peak is detected at 500 °C. The low temperature loss peak results from excess water that evaporates in the sample, the medium temperature loss peak results from the decomposition of the organic matter of the samples, the formation of volatile substances, and the high temperature loss peak most likely attributed to the fixed carbon combustion in coal [21, 22].

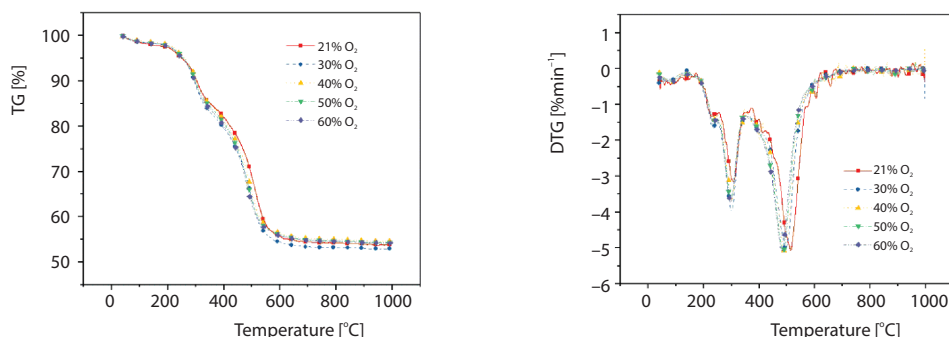


**Figure 3. The TG and DTG curves of different oxygen concentrations;**  
(a) TG curve, (b) DTG curve

The DTG curve shows that the second loss peak gradually increases as the oxygen concentration increases, but this peak does not greatly influence the temperature of the loss peak. However, the third loss peak does not change with oxygen concentration, and the temperature of the loss peak decreases as the oxygen concentration increases. An increase in oxygen concentration can increase the combustion rate of volatile substances and decrease the combustion temperature of fixed carbon. No significant influence on the combustion temperature and the combustion speed of fixed carbon is noted. However, the combustion temperature and fixed carbon combustion rate are not significantly affected.

Ignition temperature,  $T_i$ , and burnout temperature,  $T_b$ , in CG and biomass combustion are obtained through TG-DTG-combined definition method [23, 24]. The combustion performance is evaluated with the comprehensive combustion index  $S$  which encompasses the igni-

tion temperature, the combustion rate, and the burnout temperature [25]. The larger  $S$  is, the better the combustion performance will be.  $S$  can be described [26]:

$$S = \frac{\left(\frac{dw}{dt}\right)_{\max} \left(\frac{dw}{dt}\right)_{\text{aver}}}{T_i^2 T_f} \quad (1)$$

where  $T_i$  and  $T_f$  [°C] are the ignition temperature and burnout temperature, respectively, and  $(dw/dt)_{\max}$  and  $(dw/dt)_{\text{aver}}$  [%min<sup>-1</sup>] – the maximum burning rate of the sample and the average burn rate of the sample, respectively.

The variations in  $T_i$ ,  $T_f$ , and  $S$  with oxygen concentration are, respectively shown in figs. 4 and 5.

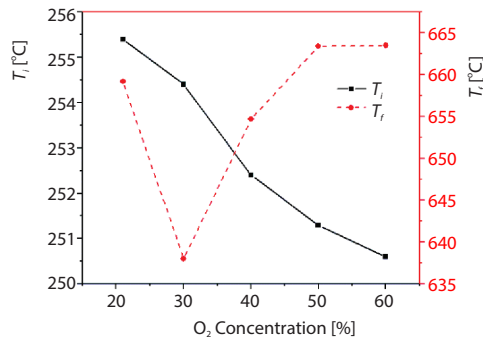


Figure 4. Curve of  $T_i$  and  $T_f$

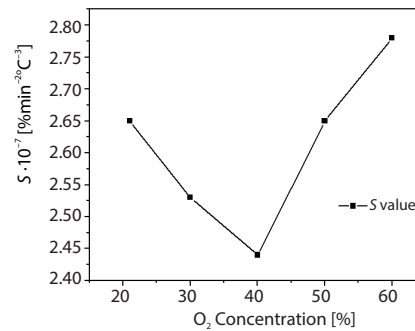


Figure 5. Curve of  $S$

The  $T_i$  of the mixed sample decreases as the oxygen concentration increases, fig. 4. As the oxygen concentration increases, the oxidation capacity of atmosphere increases, the CO<sub>2</sub> concentration in the atmosphere decreases, and the total specific heat capacity of the atmosphere decreases. As a result, the propagation velocity and diffusion rate of the sample flame increase, and the  $T_i$  decreases. The  $T_f$  of the sample decreases initially and then increases when the oxygen concentration increases. The lowest  $T_f$  is when the oxygen concentration is 30% and basically remains unchanged after the oxygen concentration is over 50%. Therefore, this finding indicates that the change in oxygen concentration influences the low oxygen atmosphere and can improve the burnout characteristics of the sample when the oxygen concentration is 30%.

The  $S$  of the sample initially decreases and subsequently increases as the oxygen concentration increases, fig. 5. The oxygen concentration increases from 21-60%, and the maximum and minimum  $S$  are both  $0.35 \cdot 10^{-7} \% / (\text{min}^2 \text{°C}^{-3})$ , which can be determined through numerical analysis. Therefore, oxygen concentration has no great influence on the comprehensive combustion performance of the mixed CG and biomass samples.

#### Analysis of DSC characteristics

The DSC curves of the mixed samples with different oxygen concentrations are shown in fig. 6.

Figure 6 shows that the DSC curve of the sample is substantially coincident before 280 °C, indicating that

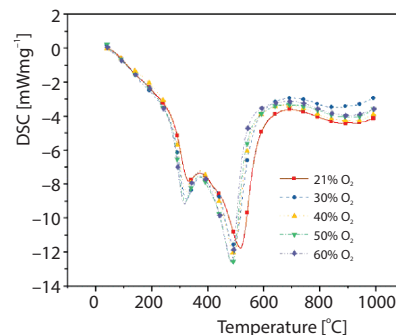


Figure 6. The DSC curves of different oxygen concentrations

the oxygen concentration does not have a large effect on the exothermic heat of the sample when the temperature is lower than 280 °C. The influence of oxygen concentration on the exothermic heat of the sample is greater than that after the temperature exceeds 280 °C, and the first exothermic peak of DSC increases as the oxygen concentration increases. The first exothermic peak of the sample DSC curve is due to the combustion of the volatiles of the sample. This result indicates that an increase in oxygen concentration can promote the combustion of volatiles in the sample. However, the second exothermic peak of the DSC sample does not change as the oxygen concentration increases. Table 3 shows the DSC curve characteristic parameters.

**Table 3. The DSC curve characteristic parameters of the samples with different oxygen concentrations**

O <sub>2</sub> concentration [%]	First peak temperature [°C]	First peak heat release [mWmg <sup>-1</sup> ]	Second peak temperature [°C]	Second peak heat release [mWmg <sup>-1</sup> ]	Total heat release [Jg <sup>-1</sup> ]
21	331.6	7.81	515.9	11.76	6524
30	323.3	8.90	492.6	11.57	6445
40	323.1	8.43	492.2	12.06	6346
50	319.3	9.06	485.5	12.65	6921
60	316.9	9.17	482.2	12.54	6585

Both exothermic peak temperatures of the mixed samples decrease when the oxygen concentration increases, tab. 3. The change in the temperature of the two exothermic peaks significantly reduces after the oxygen concentration is higher than 30%. After the oxygen concentration is higher than 30%, the change in oxygen concentration slightly influences the heat release of the sample. The heat release of the first exothermic peak increases as the oxygen concentration increases. However, the second peak of exothermic heat release is relatively stable, and no significant change is noted as the oxygen concentration increases. This finding shows that the improvement of oxygen concentration is more obvious on the first exothermic peak. The total heat release of the sample increases when the oxygen concentration increases, indicating that an appropriate oxygen concentration can better promote the heat release of the sample.

#### *Combustion tests with different biomass contents*

Combustion tests were performed on the mixed samples of pure CG, 10% CS/90% CG (10% CS), 20% CS/80% CG (20% CS), 30% CS/70% CG (30% CS), 40% CS/60% CG (40% CS), and 50% CS/50% CG, respectively, under a 30% oxygen concentration O<sub>2</sub>/CO<sub>2</sub> atmosphere.

#### *Analysis of TG and DTG characteristics*

Figure 7 shows the TG and DTG curves of the samples with different biomass contents. Figure 7 illustrates that the mixed sample of CG and biomass has three obvious weight loss peaks on the DTG curve, whereas the combustion of CG is relatively simple, and only one weight loss peak appears. The CG shows a slight weight gain before a rapid weight loss occurs. An uneven force field is noted on the surface of the CG. Oxygen atoms in the atmosphere exchange electrons with the surface of the CG, transfer, or share the adsorption of chemical bonds as temperature increases [27]. The SEM and energy spectrum analysis of CG show that more metal elements are found in the CG. Moreover, the volatile matter and moisture content of CG are low. At this time, the evaporation of water and volatile matter is insufficient to compensate

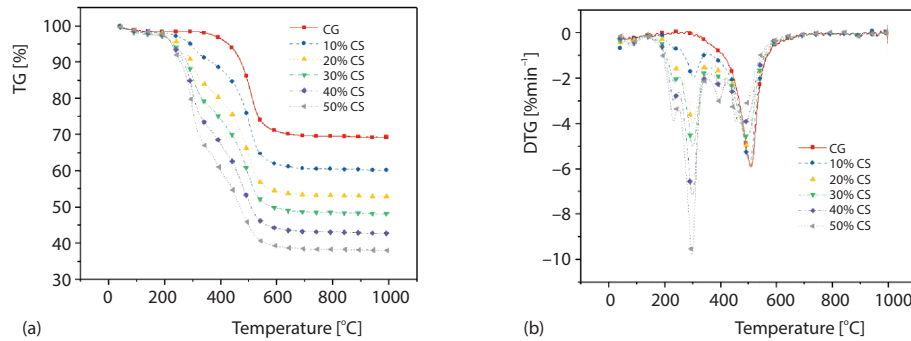


Figure 7. The TG and DTG curves of different biomass contents; (a) TG curve, (b) DTG curve

for the weight gain of oxidation between metal elements and oxygen in the air. As a result, the TG curve increases. However, the addition of the biomass mixed samples masks the weight gain of CG, and the evaporation rate of water and volatility are much higher than that of heavy metal elements in CG because of the high volatile content in biomass.

The total and maximum weight loss rates of the sample increase, whereas the fixed carbon burning weight loss peak decreases and shifts to a lower-temperature zone as the biomass content increases. This finding is due to an increase in the biomass content, resulting in an increase in the total volatile content of the sample and a decrease in the total fixed carbon content. The biomass burns first and releases a great amount of heat after it is added to the biomass. The temperature at the initial stage of combustion increases, and the combustion of CG is promoted so that the mixed sample is shifted to a lower-temperature zone in the fixed carbon combustion stage.

The variations in  $T_i$ ,  $T_f$ , and  $S$  with oxygen concentration are, respectively, shown in figs. 8 and 9.

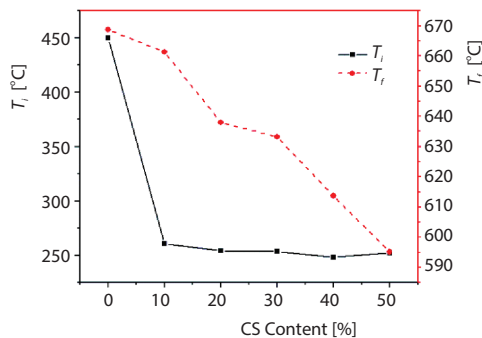


Figure 8. Curve of  $T_i$  and  $T_f$

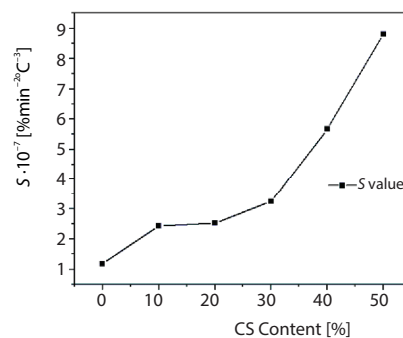


Figure 9. Curve of  $S$

The CG has a high  $T_i$  when it is burned alone, as shown in fig. 8. The low volatile matter content in CG, and the high fixed carbon content is determined through the industrial analysis of CG. Therefore, fixed carbon combustion is the main reaction stage of CG, and its own volatile combustion does not well ignite the combustion of fixed carbon, thus, CG has a high  $T_i$ . The addition of biomass can quickly reduce the  $T_i$  of the sample. The  $T_i$  of the sample initially decreases and subsequently increases as the biomass content increases. The minimum

value is obtained at a biomass content of 40%. The  $T_f$  decreases monotonously as the biomass content increases. The maximum weight loss temperature of the sample occurs in the fixed carbon combustion stage when the biomass content is less than 20%, and the maximum weight loss temperature increases as the biomass content increases. However, the maximum weight loss temperature of the sample appears in the volatile combustion stage when the biomass content is higher than 20%, and the maximum weight loss temperature decreases as the biomass content further increases.

The  $S$  of CG is low, as shown in fig. 9, indicating that CG has poor performance when it is burned alone. However,  $S$  rapidly increases after the biomass is added. The  $S$  of the sample increases only by  $0.1 \cdot 10^{-7}/(\text{min}^2\text{C}^3)$  when the biomass content increases from 10% to 20%. However,  $S$  increases by  $3.14 \cdot 10^{-7}/(\text{min}^2\text{C}^3)$  when the biomass content increases from 40% to 50%. As the same biomass content increases, the higher the biomass content is, the more obvious the effect of increasing  $S$  of the sample will be. A higher biomass content more effectively promotes  $S$  of the sample.

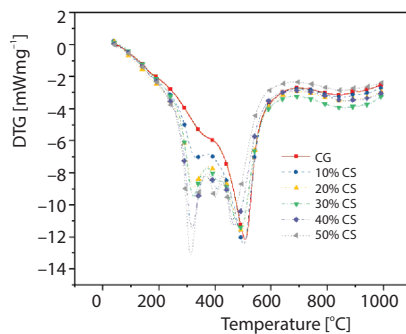


Figure 10. The DSC curves of different biomass contents

#### Analysis of DSC characteristics

Figure 10 shows the DSC curve of different biomass content samples. During the combustion of CG, a *shoulder belt* and an obvious exothermic peak that are around 380 °C and 500 °C appear in the DSC curve, respectively, as shown in fig. 10. Two significant exothermic peaks form in the mixed samples after the biomass is added. These two obvious exothermic peaks are caused by volatile combustion and fixed carbon combustion combined with DTG curve analysis, respectively. Moreover, the peaks of the two exothermic peaks differ as the biomass contents vary. Table 4 shows the DSC curve characteristic parameters.

Table 4. The DSC curve characteristic parameters of the samples with different CS contents

CS content [%]	First peak temperature [°C]	First peak heat release [mWmg <sup>-1</sup> ]	Second peak temperature [°C]	Second peak heat release [mWmg <sup>-1</sup> ]	Total heat release [Jg <sup>-1</sup> ]
CG	–	–	505.9	12.14	5334
10	331.3	7.06	501.4	12.44	6041
20	323.3	8.90	492.6	11.57	6445
30	322.6	9.47	488.8	11.38	6534
40	317.6	11.43	468.0	11.24	7044
50	312.8	13.05	458.1	11.23	7351

Note: the – indicates that the first peak of CS does not exist.

The temperature of the first exothermic peak of the mixed DSC sample moves toward the low temperature region, and the amount of heat release gradually increases when the biomass content increases, tab. 4. The addition of the biomass reduces the temperature of the second exothermic peak of CG. The higher the biomass content is, the lower the temperature will be. The combustion of biomass volatiles can promote the combustion of CG fixed carbon after the biomass is added, and the higher the biomass content is, the more obvious the promotion effect will be. The maximum exotherm occurs when the second exothermic peak is less than 40%

of the biomass content, indicating that the fixed carbon combustion of the sample dominates the reaction at this stage. However, the maximum exothermic peak appears after the first exothermic peak has a biomass content of more than 40%. As the biomass content further increases, the total volatile content of the sample increases, and the evaporative combustion of the volatile samples begins to dominate the combustion process. The higher the biomass content is, the greater the total heat release of the sample will be, tab. 4. Biomass has a higher calorific value than CG, which is known from the heating value of cartridge. As a result, it favors the higher biomass content of the mixed sample and the greater total amount of heat released.

### **Kinetic analysis**

In this study, the kinetic parameters of the activation energy of different oxygen concentrations and different biomass contents are determined via the iso-conversional Flynn-Wall-Ozawa (FWO) integration method. The FWO method belongs to the multiscan rate method, which is used to analyze the test results under different heating rates [21, 28, 29]. The FWO method does not involve the reaction mechanism function in the solution process and can obtain the reliable activation energy  $E$ -value. The kinetic parameter can be described [30]:

$$\ln \beta = \ln \left[ \frac{AE}{G(a)R} \right] - 5.331 - 1.052 \frac{E}{RT} \quad (2)$$

where  $\beta$  [ $\text{Kmin}^{-1}$ ] is a constant heating rate during combustion,  $A$  [ $\text{min}^{-1}$ ] – the pre-exponential factor,  $E$  [ $\text{kJmol}^{-1}$ ] – the activation energy,  $G(a)$  – the conversion rate function and is constant under the same conversion rate,  $R$  [ $8.314 \text{ Jmol}^{-1}\text{K}^{-1}$ ] – the gas constant, and  $T$  [ $\text{K}$ ] – the absolute temperature of function.

The conversion rate can be described [30]:

$$a = \frac{w_0 - w_t}{w_0 - w_f} 100\% \quad (3)$$

where  $w_0$  and  $w_f$  [%] are the mass fractions of the sample at the beginning and end of mass loss, respectively, and  $w_t$  [%] is the mass fraction of the sample at time  $t$ .

According to eq. (2), a plot of  $\ln \beta$  against  $1/T$  is a straight line. Based on the slope of line, we can estimate apparent activation energy,  $E$ , of the sample in different oxygen concentrations and different biomass contents at various  $a$  conversions. In consideration of the water evaporation and heat transfer of the sample effects [31], the conversion rates selected in this study range from 0.2-0.8.

Under the condition that the heating rates are 10, 15, and 20 °C per minute, respectively, and the biomass content is 20%, the kinetic parameters of samples with different oxygen concentrations are determined. The fitting image is shown in fig. 11. The active energies calculated are listed in tab. 5.

Table 5 shows that the activation energy of the samples initially decrease and subsequently increase as the sample conversion rate increases under different oxygen concentrations. At the initial combustion stage, the sample needs to absorb more heat to make the internal volatile devolatilization and combustion, so the activation energy is high. The reaction can be carried out without an external environment providing more heat for the subsequent reaction because a large amount of heat can be generated for the subsequent reaction after the sample begins to burn. Herein, the activation energy decreases as the conversion rate increases. As the reaction further proceeds, the volatiles of the sample burn out, and the fixed carbon of the

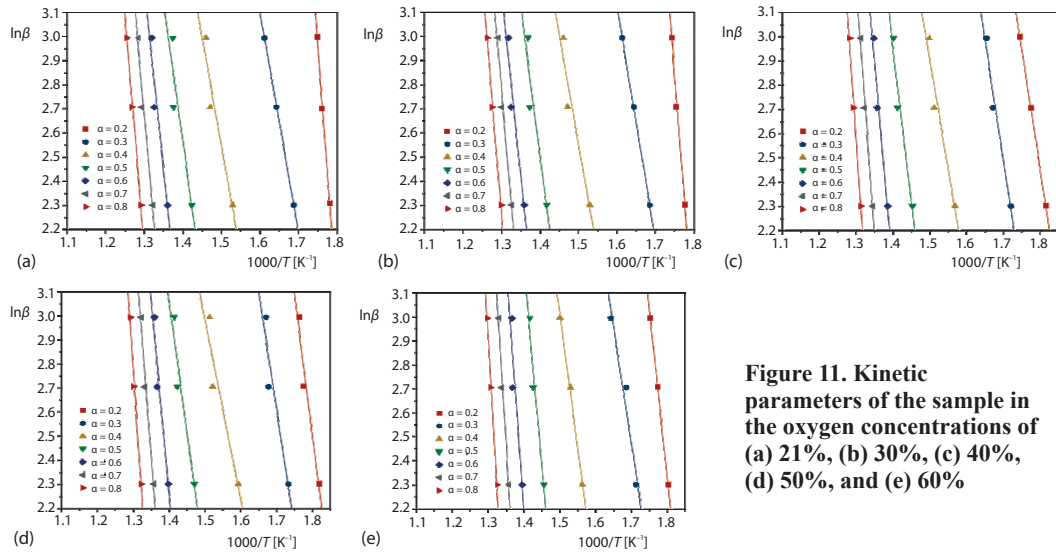


**Figure 11.** Kinetic parameters of the sample in the oxygen concentrations of (a) 21%, (b) 30%, (c) 40%, (d) 50%, and (e) 60%

**Table 5.** Kinetic parameters of the sample in different oxygen concentrations

$a$	21% O <sub>2</sub>		30% O <sub>2</sub>		40% O <sub>2</sub>		50% O <sub>2</sub>		60% O <sub>2</sub>	
	$E$ [kJmol <sup>-1</sup> ]	$R^2$								
0.2	191.00	0.992	180.44	0.995	95.43	1.000	99.43	0.954	110.37	1.000
0.3	72.45	1.000	73.08	0.999	78.94	0.977	76.72	0.907	76.98	0.947
0.4	71.22	0.929	71.51	0.927	71.38	0.944	59.14	0.898	88.26	0.996
0.5	91.11	0.858	98.25	0.901	100.82	0.953	85.77	0.918	130.64	0.968
0.5	119.01	0.922	122.41	0.920	137.73	0.961	125.18	0.949	164.30	0.861
0.7	141.67	0.965	141.05	0.976	161.17	0.975	153.40	0.961	187.78	0.953
0.8	150.04	0.987	176.71	0.992	174.16	0.985	170.22	0.970	206.53	0.983
Average	119.50	0.950	123.35	0.959	117.09	0.971	109.98	0.937	137.84	0.958

Note: The  $R^2$  indicates the related coefficient

sample begins to coke. The combustion reaction transitioned from a homogeneous reaction a heterogeneous one, which requires a large amount of heat to be absorbed, so the activation energy increases.

When the conversion rate is 0.2, the activation energy gradually decreases as the oxygen concentration increases. When the conversion rate is high, the activation energy increases as the oxygen concentration increases. The initial combustion reaction mainly involves volatile release, combustion, and a dynamic control area [32]. As such, as the oxygen concentration increases, the oxidation ability of the combustion atmosphere is enhanced, and the combustion reaction is promoted. However, when the conversion rate is high, the reaction temperature of the sample is high. At a higher temperature, a C-CO<sub>2</sub> solid-gas heterogeneous reaction occurs between CO<sub>2</sub> and part of the fixed carbon. The lower the oxygen concentration is, the higher the CO<sub>2</sub> content will be. Furthermore, carbon and CO<sub>2</sub> can be more easily fixed. As a result, the activation energy of the reaction increases as the oxygen concentration increases.

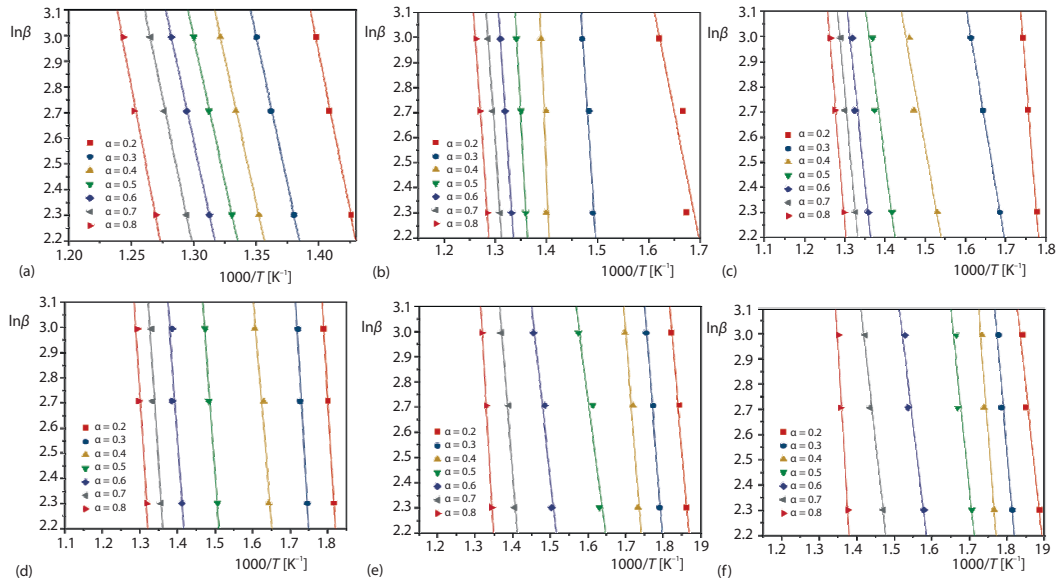


**Figure 12. Kinetic parameters of the sample in the biomass contents of (a) 0% (CG), (b) 10%, (c) 20%, (d) 30%, (e) 40%, and (f) 50%**

**Table 6. Kinetic parameters of the sample in the different biomass contents**

$\alpha$	CG		10% CS		20% CS		30% CS		40% CS		50% CS	
	$E$ [kJmol <sup>-1</sup> ]	$R^2$										
0.2	194.44	0.999	122.01	0.756	180.44	0.995	197.73	1.000	139.41	0.986	108.89	0.923
0.3	181.32	0.999	251.71	0.929	73.08	0.999	196.33	0.959	133.38	0.982	146.11	0.956
0.4	178.10	0.999	383.49	0.673	71.51	0.927	142.56	0.948	130.29	0.951	152.02	0.940
0.5	177.83	1.000	291.16	0.988	98.25	0.901	165.66	0.986	91.18	0.910	113.81	0.902
0.6	179.89	1.000	248.38	1.000	122.41	0.920	165.84	0.837	108.68	0.938	97.71	0.928
0.7	189.36	0.998	213.39	0.997	141.05	0.976	185.30	0.884	154.02	0.970	108.02	0.966
0.8	205.66	0.987	219.38	0.989	176.71	0.992	191.76	0.919	205.57	0.997	209.93	0.927
Average	186.66	0.997	247.07	0.905	123.35	0.959	177.88	0.933	137.50	0.962	133.78	0.935

Note: The  $R^2$  indicates the related coefficient

The kinetic parameters of the samples with different biomass contents are obtained at an oxygen concentration of 20%. The fitting curve and fitting results are shown in fig. 12 and tab. 6, respectively.

When the conversion rate is low, the activation energy of CG reaction alone is high, and the activation energy can be rapidly reduced after a small amount of biomass is added, tab. 6. However, the activation energy does not further decrease as the biomass content increases. At biomass contents of 10% and 50%, the activation energy increases during the conversion rate from 0.2-0.4. The biomass cannot cause the combustion of CG because the biomass is low. The CG also needs more heat from the outside to reach the combustion conditions, therefore, the activation energy increases. However, as the biomass content increased, the total volatilization of the sample increased. Before the sample is converted to 0.4, volatilization is main-

ly carried out. The process requires more energy from the outside, and the activation energy increases. At the end of combustion, the change in the biomass content does not significantly change the activation energy, which stabilizes at about 200 kJ/mol. This result indicates that biomass content has no significant influence on the end of combustion of the mixed sample. At the end of combustion burns, the fixed carbon combustion reaction was mainly taken place, so the biomass content at the end of combustion does not have a significant effect.

## Conclusions

In this study, the combustion and kinetic characteristics of the sample under different oxygen concentrations and biomass contents were determined through TG and FWO integration method. Based on our results, the following conclusions were drawn.

- As the oxygen concentration increased, the oxidizing ability of combustion atmosphere increased. As a result, the evaporation rate of the sample volatile matter increased, the temperature of fixed carbon combustion, ignition and DSC exothermic decreased, with increase of oxygen concentration, under different oxygen concentration O<sub>2</sub>/CO<sub>2</sub> atmosphere.
- As the biomass content increased, the total and the maximum weight loss rates of the sample gradually increased, whereas the weight loss peak of the fixed carbon combustion gradually decreased and shifted to lower temperature zone. The ignition temperature initially decreased and subsequently increased. The burnout temperature and the exothermic peak temperature gradually decreased, whereas the comprehensive combustion index gradually increased when the biomass content increased.
- As the sample conversion and combustion occurred via a homogeneous reaction transition a heterogeneous reaction, the activation energy of the sample initially decrease and subsequently increase. At the beginning of combustion, the activation energy gradually reduced as the oxygen concentration increased. On the contrary, the reaction activation energy increased as the oxygen concentration increased. At the initial stage of the reaction, the activation energy of CG combustion is relatively high, and the activation energy can be rapidly reduced after a small amount of biomass was added. The biomass content had no significant influence on the activation energy of the samples at the end of combustion.

## Acknowledgment

This work was financially supported by the Natural Science Foundation of China (51466010), Research Program of Science and Technology at Universities of Inner Mongolia Autonomous Region (No. NJZY18082).

## References

- [1] Hadjipaschalis, I., *et al.*, Assessment of Oxyfuel Power Generation Technologies, *Renewable and Sustainable Energy Reviews*, 13 (2009), 9, pp. 2637-2644
- [2] Hodzic, N., *et al.*, Concept of Co-Firing Coal with Biomass and Natural Gas – On Track of Sustainable Solution for Future Thermal Power Plants, *Thermal Science*, 20 (2016), 4, pp. 1171-1184
- [3] Toftegaard, M. B., *et al.*, Oxy-Fuel Combustion of Solid Fuels, *Progress in Energy and Combustion Science*, 36 (2010), 5, pp. 581-625
- [4] Gao, Z., *et al.*, Thermogravimetric Test Study on Combustion Characteristics of Mixed Coal, *Journal of Power Engineering*, (2002), 03, pp. 1764-1767+1749
- [5] Nimmo, W., *et al.*, The Effect of O<sub>2</sub> Enrichment on NO<sub>x</sub> Formation in Biomass Co-Fired Pulverised Coal Combustion, *Fuel*, 89 (2010), 10, pp. 2945-2952
- [6] Chen, L., *et al.*, Oxy-Fuel Combustion of Pulverized Coal: Characterization, Fundamentals, Stabilization and CFD Modelling, *Progress in Energy and Combustion Science*, 38 (2012), 2, pp. 156-214

- [7] Demirbas, A., Combustion Characteristics of Different Biomass Fuels, *Progress in Energy and Combustion Science*, 30 (2004), 2, pp. 219-230
- [8] Akinrinola, F. S., et al., Characterization of Selected Nigerian Biomass for Combustion and Pyrolysis Applications, *Energy and Fuels*, 28 (2014), 6, pp. 3821-3832
- [9] Cepic, Z. M., Nakomcic-Smaragdakis, B. B., Experimental Analysis of the Influence of Air-Flow Rate on Wheat Straw Combustion in a Fixed Bed, *Thermal Science*, 21 (2017), 3, pp. 1443-1452
- [10] Tahmasebi, A., et al., Thermogravimetric Study of the Combustion of Tetraselmis Suecica Microalgae and its Blend with a Victorian Brown Coal in O<sub>2</sub>/N<sub>2</sub> and O<sub>2</sub>/CO<sub>2</sub> Atmospheres, *Bioresource Technology*, 150 (2013), Dec., pp. 15-27
- [11] Kayahan, U., Ozdogan, S., Oxygen Enriched Combustion and Co-Combustion of Lignites and Biomass in a 30 kW<sub>th</sub> Circulating Fluidized Bed, *Energy*, 116 (2016), Part 1, pp. 317-328
- [12] Kazanc, F., et al., Emissions of NO<sub>x</sub> and SO<sub>2</sub> from Coals of Various Ranks, Bagasse, and Coal-Bagasse Blends Burning in O<sub>2</sub>/N<sub>2</sub> and O<sub>2</sub>/CO<sub>2</sub> Environments, *Energy Fuels*, 25 (2011), 7, pp. 2850-2861
- [13] Riaza, J., et al., Ignition and NO Emissions of Coal and Biomass Blends under Different Oxy-fuel Atmospheres, *Energy Procedia*, 37 (2013), Dec., pp. 1405-1412
- [14] Zhou, C., et al., Partitioning and Transformation Behavior of Toxic Elements During Circulated Fluidized Bed Combustion of Coal Gangue, *Fuel*, 135 (2014), 11, pp. 1-8
- [15] Liu, H., Liu, Z., Recycling Utilization Patterns of Coal Mining Waste in China, *Resources Conservation and Recycling*, 54 (2010), 12, pp. 1331-1340
- [16] Querol, X., et al., Environmental Characterization of Burnt Coal Gangue Banks at Yangquan, Shanxi Province, China, *International Journal of Coal Geology*, 75 (2008), 2, pp. 93-104
- [17] Zhang, Y., et al., Interactions of Coal Gangue and Pine Sawdust During Combustion of Their Blends Studied using Differential Thermogravimetric Analysis, *Bioresour Technol*, 214 (2016), Aug., pp. 396-403
- [18] Chen, Y., Experimental Study on the Pyrolysis and Combustion Characteristics of Biomass and Coal Gangue (in Chinese), Ph. D. thesis, Chongqing University, Chongqing, China, 2007
- [19] Song, C., et al., Orthogonal Experiment Analysis of Coal Gangue and Corn Straw Mixed Burning under Considering Multiple Factors, *Proceedings*, 2<sup>nd</sup> Int. Con. on Physics, Mathematics and Statistics, Hangzhou, China, Journal of Physics: Conference Series, Vol. 1324, 012065, 2019
- [20] Song, C., et al., Analysis of Mixed Combustion Characteristics of Coal Gangue and Biomass (in Chinese) *Renewable Energy Resources*, 37 (2019), 12, pp. 1764-1769
- [21] Duan, L., et al., Combustion Characteristics and Kinetic Analysis of Pulverized Coal under O<sub>2</sub>/CO<sub>2</sub> Atmosphere, *Journal of Combustion Science and Technology*, 24 (2018), 03, pp. 223-231
- [22] Biagini, E., et al., Devolatilization Rate of Biomasses and Coal-Biomass Blends: An Experimental Investigation, *Fuel*, 81 (2002), 8, pp. 1041-1050
- [23] Li, Q., et al., Comparison of Pulverized Coal Combustion in Air and in O<sub>2</sub>/CO<sub>2</sub> Mixtures by Thermo-Gravimetric Analysis, *Journal of Analytical and Applied Pyrolysis*, 85 (2009), 1, pp. 521-528
- [24] Gong, Z., et al., Orthogonal Test Analysis of mixed Burning of Coal Gangue and Corn Stalk (in Chinese), *Journal of Inner Mongolia University of Technology (natural science edition)*, (2019), 04, pp. 261-268
- [25] Chen, X., et al., Thermal Analyses of the Lignite Combustion in Oxygen-Enriched Atmosphere, *Thermal Science*, 19 (2015), 3, pp. 801-811
- [26] Huang, X., et al., Combustion Characteristics of Fine- and Micro-Pulverized Coal in the Mixture of O<sub>2</sub>/CO<sub>2</sub>, *Energy and Fuels*, 22 (2008), 6, pp. 3756-3762
- [27] Li, J., et al., Study on Combustion Characteristics of Coal Gangue and Vulcanized Nitrile Butadiene Rubber (in Chinese), *Renewable Energy Resources*, 36 (2018), 11, pp. 1581-1587
- [28] Zhang, Y.-F., et al., Oxygen-Enriched Combustion of Lignite, *Thermal Science*, 19 (2015), 4, pp. 1389-1392
- [29] Zou, S., et al., Pyrolysis Characteristics and Kinetics of the Marine Microalgae *Dunaliella Tertiolecta* using Thermogravimetric Analyzer, *Bioresource Technology*, 101 (2010), 1, pp. 359-365
- [30] Gil, M. V., et al., Thermal Behaviour and Kinetics of Coal/Biomass Blends during Co-Combustion, *Biore-sour Technol*, 101 (2010), 14, pp. 5601-5608
- [31] Jankovic, B., et al., A Kinetic Study of Non-Isothermal Decomposition Process of Anhydrous Nickel Nitrate under Air Atmosphere, *Physica B-Condensed Matter*, 404 (2009), 16, pp. 2263-2269
- [32] Xu, T., Hui, S., *Combustion Science* (in Chinese), China Machine Press, Beijing, China, 2017